Phenotypic characterization of glioblastoma identified through shape descriptors

Ahmad Chaddad*, Christian Desrosiers, Matthew Toews
Laboratory for Imagery, Vision and Artificial Intelligence, Ecole de Technologie Superieure, Montreal, Qc, H3C1K3, Canada

ABSTRACT

This paper proposes quantitatively describing the shape of glioblastoma (GBM) tissue phenotypes as a set of shape features derived from segmentations, for the purposes of discriminating between GBM phenotypes and monitoring tumor progression. GBM patients were identified from the Cancer Genome Atlas, and quantitative MR imaging data were obtained from the Cancer Imaging Archive. Three GBM tissue phenotypes are considered including necrosis, active tumor and edema/invasion. Volumetric tissue segmentations are obtained from registered T1-weighted (T1-WI) post-contrast and fluid-attenuated inversion recovery (FLAIR) MRI modalities. Shape features are computed from respective tissue phenotype segmentations, and a Kruskal-Wallis test was employed to select features capable of classification with a significance level of $p < 0.05$. Several classifier models are employed to distinguish phenotypes, where a leave-one-out cross-validation was performed. Eight features were found statistically significant for classifying GBM phenotypes with $p < 0.05$, orientation is uninformative. Quantitative evaluations show the SVM results in the highest classification accuracy of 87.50%, sensitivity of 94.59% and specificity of 92.77%. In summary, the shape descriptors proposed in this work show high performance in predicting GBM tissue phenotypes. They are thus closely linked to morphological characteristics of GBM phenotypes and could potentially be used in a computer assisted labeling system.

Keywords: Classification, GBM, MRI, Shape feature,

1. INTRODUCTION

Glioblastoma is the most aggressive primary brain tumor [1]. Because of its resistance to conventional therapies, the life expectancy of GBM patients rarely exceeds two years from the initial diagnosis, with a median survival time of 12.6 months [2,3]. Despite the various lines of treatments available, e.g. combinations of surgery, radiation therapy and/or chemotherapy, the prognosis for GBM cases remains poor.

During its aggressive proliferation, a GBM affects the morphological appearance of surrounding regions in the brain, and generally develops into an irregular shape observable by MRI. In this process, sub-tumors are generated from the main GBM tumor, which separates in different clusters of cells [4]. These clusters then grow separately, depending on fluctuations in local oxygen and nutrient supply at a macroscopic scale [4,5]. Moreover, GBMs generally develop along white matter regions and, less commonly, along the edge of cerebrospinal fluid-filled regions [6]. This irregular growth process leads to a wide variety of complex tumor shapes [7].

The shape of the core tumor is generally extracted using a semi-automatic segmentation method, which allows a more detailed and controlled segmentation than the fully automatic approaches [8,9]. To achieve a maximum accuracy, manual segmentation is often performed using a specialized tool, e.g. 3D Slicer [10,11]. This step may improve the quantitative assessment of the morphological aspects of GBM growth. In this context, a number of clinical features have been shown to be associated with GBM patients. For example, Karnofsky Performance Status (KPS) and age [12,13] have been investigated for predicting GBM survival time. Gross total resection is associated with a better prognosis [12]. Furthermore, genetic information has been shown to contain predictive biomarkers associated with GBM [14], and gene expression has been associated with patient survival and response to aggressive therapy [15,16]. Imaging features have also been proposed as potential predictors of survival time [13,17], including standardized lexicons of image features derived from MRI [18,19]. However, the utility of shape features for discriminating between GBM phenotypes is still limited, even if the shape features represent the abnormalities level of the GBM tumor.

This work focuses on identifying clinically relevant GBM tissue phenotypes based on shape descriptors analysis. And, we seek to demonstrate a GBM sub-classification based on shape descriptors analysis that is both predictive and prognostic.

The paper is organized as follows. Section 2 starts with the materials of GBM data, and then details of the registration, segmentation on 3D Slicer tool, the proposed descriptors and classification scheme. In Section 3, we present and discuss the experimental results. Finally, we provide concluding remarks and possible extensions.

2. MATERIALS AND METHODS

Figure 1 illustrates the flowchart of the proposed method. In the first step, T1−WI and FLAIR volumes are aligned using a rigid registration process in 3D Slicer software platform [10]. Segmentation is then applied to the registered volumes to delineate the three GBM phenotypes. In the third step, active tumor/invasion and necrotic tissues are extracted from T1−WI and edema tissues from FLAIR. A set of nine shape descriptors is computed slice-by-slice for each phenotype. Finally, classifier models are trained and evaluated using these descriptors to predict the GBM phenotypes.

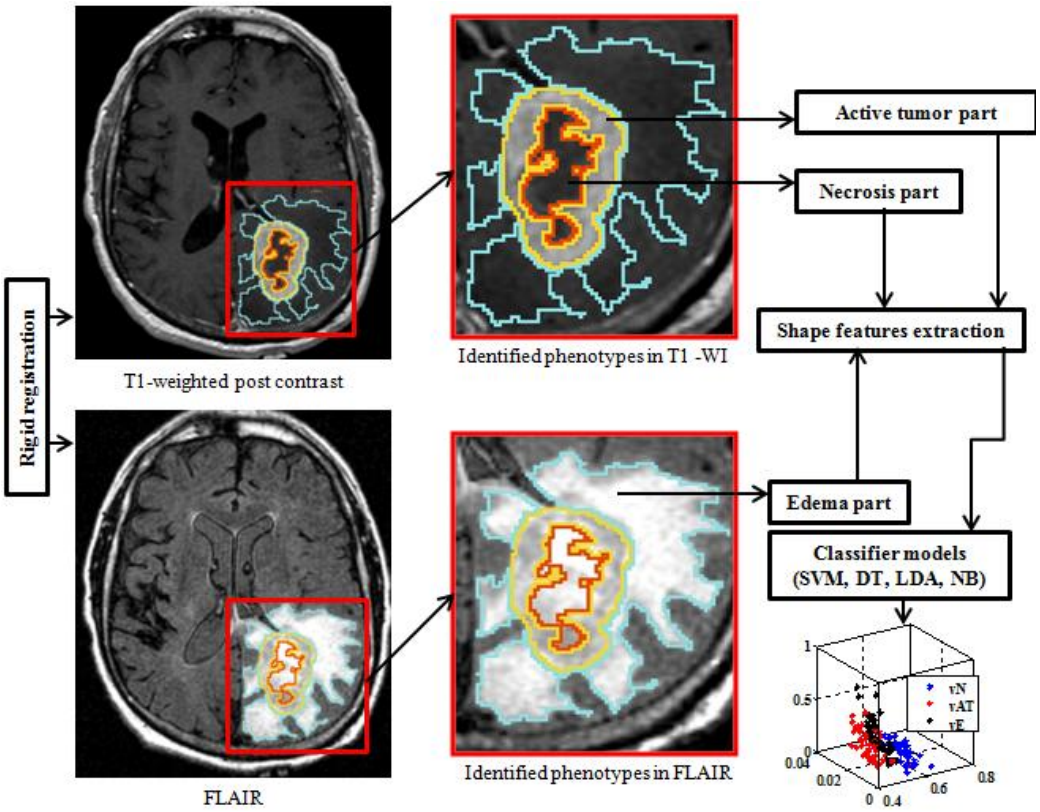

Figure 1. Block diagram showing the extraction of shape descriptors and classification of GBM tissue phenotypes.

2.1 Patient and imaging data

Data of 42 patients were obtained from the Cancer Genome Atlas (TCGA, http://cancergenome.nih.gov/). The GBM data were acquired prior to treatment from brain tumor patients that were subsequently diagnosed as GBM. Patient data were visually assessed as having sufficient quality and as containing the relevant tissue phenotypes (necrosis, contrast enhancement/active tumor and edema/invasion), using the 3D Slicer software for visualization and segmentation. For each patient, two MR imaging sequences were considered: (1) T1−WI and (2) FLAIR. Image regions corresponding to different GBM phenotypes were manually labeled in each slice and validated visually by at least two radiologists. These labels then served as guide to train our algorithm for shape descriptors. All of the images where acquired at resolution 512 × 512. Registration and segmentation were then employed on GBM phenotypes for data collection.

2.2 Segmentation

Prior to segmenting the GBM phenotypes, post-contrast T1−WI and FLAIR images are automatically registered using a rigid transform model. This step is required for delineating GBM phenotypes from multiple image modalities within the same reference space. In several cases, patient data resulted in high registration error, e.g. due to non-trivial 3D rotations between images, these were excluded from experiments in order to maintain an alignment error < 2 mm. Each volume-to-volume registration required 40−45 seconds using the 3D Slicer tool. Image regions corresponding to different GBM phenotypes were then segmented manually in a slice-by-slice fashion, after which they were used as the basis for computing the shape descriptors (e.g. Figure 2). Shape descriptors for necrosis and active tumor phenotypes were computed from T1-WI intensity data, while descriptors for edema/invasion were calculated from the FLAIR sequence.

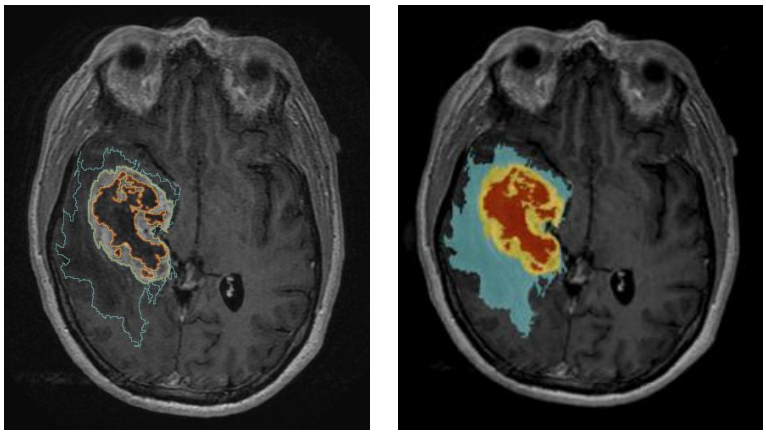

(a) (b)

Figure 2. Example of GBM phenotypes: (a) segmented phenotype by 3D Slicer, (b) necrosis, active tumor (Contrast enhancement) and edema are labeled by the red, yellow and cyan colors respectively.

2.3 Computation of shape features

We considered nine shape features for characterizing each phenotypical region, and these features are computed from 2D slices in a slice-by-slice fashion where each feature value is represented the average of the corresponding value in whole slices. A feature vector F is thus represented as follows:

$$F_{pi} = [\, f_1, f_2, f_3, f_4, f_5, f_6, f_7, f_8, f_9 \,] \quad (1)$$

where p is the index of the patient, i is the index of the tissue phenotype, e.g. necrosis ($i=1$), active tumor ($i=2$), and edema ($i=3$).

The following two-dimensional shape features are considered: area (f_1), eccentricity (f_2), equivalent diameter (f_3), filled area (f_4), extent (f_5), major (f_6) and minor (f_7) axis lengths, orientation (f_8), and perimeter (f_9). These features were chosen as they can be used to distinguish between regular and irregular shapes, indicative of GBM phenotypes. The average and standard deviation is computed for each shape parameter over all phenotype slices, in order to characterize statistical variability across GBM phenotype shapes, including potential irregularities. The driving hypothesis of our approach is that an optimal combination of these descriptors may be useful in discriminating between GBN phenotypes and predicting overall survival patient survival. The computational details of these features can be found in the region properties tool in Matlab.

2.4 Statistical analysis and classifier setting

We normalized each feature vector to zero mean and unit variance using Z-score model. The Kruskal-Wallis test was applied to assess the statistical difference of shape features among the three GBM phenotypes [20]. We employed then four different classifier techniques, namely, linear discriminant analysis (LDA) [21], naïve Bayes (NB) [22], decision trees (DT) [23], and support vector machine (SVM) [24]. Implementation details for each classifier were generally chosen to achieve optimal performance in cross validation.

Due to the limited patients number, classifier cross-validation is performed using a leave-one-out model [25], where training and testing is based on GBM phenotype labels (necrosis, active tumor and edema) and shape feature data. We report results of the classifier accuracy, sensitivity, and specificity according to the following equations:

$$Accuracy = \frac{TP+TN}{TP+FP+TN+FN} \quad (2)$$

where the true positive (*TP*) and the true negative (*TN*) rates are the number of correctly classified positive and negatives classes. The false positive (*FP*) and false negative (*FN*) are those samples which are incorrectly classified.

Sensitivity evaluates the capability of a classifier to recognize the positive class patterns. It can be expressed according to

$$Sensitivity = \frac{TP}{TP+FN} \quad (3)$$

Specificity evaluates the capability of a classifier to recognize the negative class patterns. It can be expressed by the following equation:

$$Specificity = \frac{TN}{TN+FP} \quad (4)$$

Finally, we also computed the confusion matrix to visualize the number of correct and incorrect predictions for each of GBM phenotypes.

3. EXPERIMENTAL RESULT

A dataset of 42 GBM patients (female 20; male 22; median age 61 years; mean age 58.75 years; age range from 18 to 80 years) was collected from the NCI's Cancer Imaging Archive (TCIA).

Nine shape descriptors: area (f_1), eccentricity (f_2), equivalent diameter (f_3), filled area (f_4), extent (f_5), major (f_6) and minor (f_7) axis lengths, orientation (f_8), and perimeter (f_9) have extracted from each GBM phenotypes, where the GBM phenotypes are volumes of active tumor (vAT), volumes of tumor necrosis (vN), and volumes of edema/tumor invasion (vE).

Table 1 shows the average value (and standard deviation) of the nine shape descriptors, for each GBM phenotype. Edema parts (vE) show higher value in features f_1, f_2, f_6 and f_9, while active tumor parts (vAT) show higher value in features f_3, f_5, f_7 and f_8, and necrosis parts (vN) a higher value in feature f_4. Using a Kruskal-Wallis test with significance level $p < 0.05$, we identified eight discriminative features: f_1, f_2, f_3, f_4, f_5, f_6, f_7, f_9.

Table 1. Summary of shape descriptors (average ± standard deviation)

Descriptor (features)	vN	vAT	vE	*p*
f_1: area	339.39 ± 510.6	934.12 ± 538.98	985.52 ± 580.37	< 0.001
f_2: eccentricity	0.76 ± 0.056	0.70 ± 0.077	0.79 ± 0.06	< 0.001
f_3: equivalent diameter	13.82 ± 10.08	29.84 ± 9.42	28.97 ± 9.01	0.02
f_4: filled area	0.602 ± 0.07	0.55 ± 0.075	0.512 ± 0.043	< 0.001
f_5: extent	341.85 ± 513.44	1309.3 ± 810.52	1023.8 ± 616.34	< 0.001
f_6: major axis length	20.09 ± 12.91	47.001 ± 17.13	50.433 ± 14.95	< 0.001
f_7: minor axis length	11.82 ± 8.58	32.35 ± 12.28	26.01 ± 9.16	0.01
f_8: orientation	-0.57 ± 22.3	-0.002 ± 31.67	-1.55 ± 26.88	0.65
f_9: perimeter	68.66 ± 50.84	149.13 ± 55.14	184.63 ± 67.32	< 0.001

The accuracy, sensitivity, and specificity of four classifier models, Linear Discriminant Analysis (LDA), Support Vector Machines (SVM), Decision Tree (DT) and Naive Bayes (NB), are summarized in Table 2. For the eight selected shape features, SVM obtained the best overall results per GBM phenotype with 87.50% accuracy, 94.59% sensitivity and 92.77% which is closed to LDA classifier metrics, while the DT and NB classifier was provided a limited accuracy classifier with 73.33%.

Table 2. Quantitative classification (leave-one-out cross validation) results for the eight selected shape features

Classifiers	% Accuracy	% Sensitivity	% Specificity
LDA	86.67	86.49	92.77
SVM	87.50	94.59	92.77
DT	73.33	89.19	89.16
NB	73.33	83.78	80.72

The confusion matrix shows the advantage of the shape features for identifying the necrosis (35 samples correctly classified from 37 samples which are represented the accuracy value of 94.59 %) with SVM classifier, active tumor (35 samples correctly classified from 42 sample which are represented the accuracy value of 83.33 %) and edema parts (37 samples correctly classified 41 samples which are represented 90.24 %) using linear LDA (Table 3). Moreover, the predictive accuracy of GBM phenotypes decreased in active tumor and edema parts, which represent the correlation between the shape features of active tumor and edema parts (e.g. Figure 3). Clearly, ensemble of shape features in active tumor and edema phenotype have a high correlation with value range of 0.4−0.7.

Table 3. Summary of confusion matrix for GBM phenotype classification

Classifiers	LDA			SVM			DT			NB		
Samples	vN	vAT	vE	vN	vAT	vE	vN	vAT	vE	vN	vAT	vE
vN (37)	32	5	0	35	2	0	33	1	3	31	4	2
vAT (42)	5	35	2	6	34	2	8	26	8	9	28	5
vE (41)	1	3	37	0	5	36	1	11	29	7	5	29

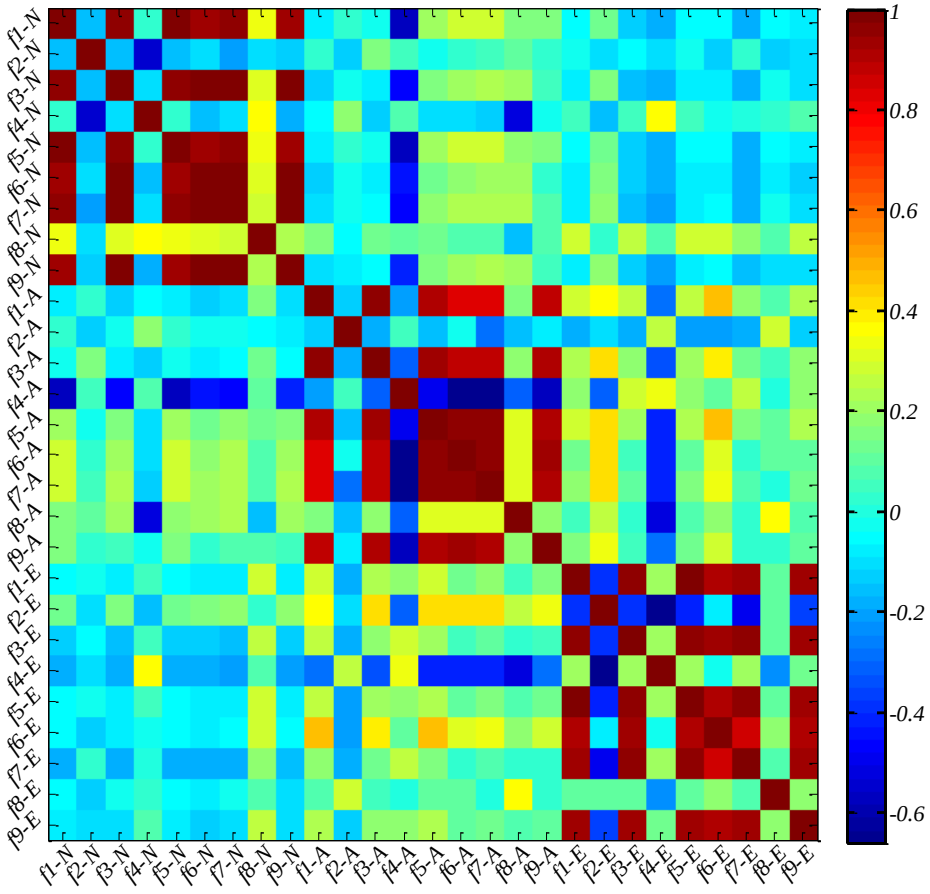

Figure 3. Heat map with correlation coefficients between shape features of GBM phenotypes: N, A, and E are the necrosis, active tumor, and edema respectively; f_1, f_2, f_3, f_4, f_5, f_6, f_7, f_8 and f_9 are the shape descriptors.

There are several potential benefits of the methods proposed in this paper. 1) They provide radiologists a tool for assessing GBM phenotypes, using 8 shape features and two MRI sequences T1−WI and FLAIR. 2) They offer an accurate quantitative approach to shape feature description from segmentations provided by a radiologist. Finally, the limited set of 8 features is simple and intuitive to understand, yet can effectively summarize shape information not easily visually observable from raw images. Also, a comparison with a previous study [26] showed that this approach can be a promising avenue for future research. Note that this work is a part of a large focus on radiomic analysis of GBM phenotypes [27–29].

4. CONCLUSIONS

We presented a novel approach using shape descriptors to classify GBM phenotypes. Preliminarily results obtained on 42 patients demonstrate the usefulness of these features in the prediction of phenotypes, with an accuracy of 87.50% when used with the SVM classifier. Future work will focus on improving the accuracy of the method by combining more feature types, e.g. gradient orientation-based descriptors such as 3D SIFT-Rank [30], and further quantifying the association with between image features and GBM patient survival.

REFERENCES

[1] Stupp, R., Hegi, M. E., Bent, M. J. van den., Mason, W. P., Weller, M., Mirimanoff, R. O.., Cairncross, J. G., "Changing Paradigms—An Update on the Multidisciplinary Management of Malignant Glioma," The Oncologist **11**(2), 165–180 (2006).

[2] Stupp, R., Mason, W. P., van den Bent, M. J., Weller, M., Fisher, B., Taphoorn, M. J. B., Belanger, K., Brandes, A. A., Marosi, C., et al., "Radiotherapy plus concomitant and adjuvant temozolomide for glioblastoma," N. Engl. J. Med. **352**(10), 987–996 (2005).

[3] Johnson, D. R., Ma, D. J., Buckner, J. C.., Hammack, J. E., "Conditional probability of long-term survival in glioblastoma," Cancer **118**(22), 5608–5613 (2012).

[4] Frieboes, H. B., Zheng, X., Sun, C.-H., Tromberg, B., Gatenby, R.., Cristini, V., "An integrated computational/experimental model of tumor invasion," Cancer Res. **66**(3), 1597–1604 (2006).

[5] Frieboes, H. B., Lowengrub, J. S., Wise, S., Zheng, X., Macklin, P., Bearer, E.., Cristini, V., "Computer Simulation of Glioma Growth and Morphology," NeuroImage **37**(Suppl 1), S59–S70 (2007).

[6] Claes, A., Idema, A. J.., Wesseling, P., "Diffuse glioma growth: a guerilla war," Acta Neuropathol. (Berl.) **114**(5), 443–458 (2007).

[7] Kim, Y., Lawler, S., Nowicki, M. O., Chiocca, E. A.., Friedman, A., "A mathematical model for pattern formation of glioma cells outside the tumor spheroid core," J. Theor. Biol. **260**(3), 359–371 (2009).

[8] Jones, T. L., Byrnes, T. J., Yang, G., Howe, F. A., Bell, B. A.., Barrick, T. R., "Brain tumor classification using the diffusion tensor image segmentation (D-SEG) technique," Neuro-Oncol., nou159 (2014).

[9] Chaddad, A., "Automated Feature Extraction in Brain Tumor by Magnetic Resonance Imaging Using Gaussian Mixture Models," Int. J. Biomed. Imaging **2015**, e868031 (2015).

[10] "3D Slicer.", <http://www.slicer.org/> (20 October 2014).

[11] Egger, J., Kapur, T., Fedorov, A., Pieper, S., Miller, J. V., Veeraraghavan, H., Freisleben, B., Golby, A. J., Nimsky, C., et al., "GBM volumetry using the 3D Slicer medical image computing platform," Sci. Rep. **3**, 1364 (2013).

[12] Michel Lacroix, D. A.-S., "A multivariate analysis of 416 patients with glioblastoma multiforme: prognosis, extent of resection, and survival," J. Neurosurg. **95**(2), 190–198 (2001).

[13] Park, J. K., Hodges, T., Arko, L., Shen, M., Iacono, D. D., McNabb, A., Bailey, N. O., Kreisl, T. N., Iwamoto, F. M., et al., "Scale to Predict Survival After Surgery for Recurrent Glioblastoma Multiforme," J. Clin. Oncol. **28**(24), 3838–3843 (2010).

[14] McDonald, K. L., Aw, G.., Kleihues, P., "Role of Biomarkers in the Clinical Management of Glioblastomas: What are the Barriers and How Can We Overcome Them?," Front. Neurol. **3** (2013).

[15] Colman, H., Zhang, L., Sulman, E. P., McDonald, J. M., Shooshtari, N. L., Rivera, A., Popoff, S., Nutt, C. L., Louis, D. N., et al., "A multigene predictor of outcome in glioblastoma," Neuro-Oncol. **12**(1), 49–57 (2010).

[16] Verhaak, R. G. W., Hoadley, K. A., Purdom, E., Wang, V., Qi, Y., Wilkerson, M. D., Miller, C. R., Ding, L., Golub, T., et al., "Integrated genomic analysis identifies clinically relevant subtypes of glioblastoma characterized by abnormalities in PDGFRA, IDH1, EGFR, and NF1," Cancer Cell **17**(1), 98–110 (2010).

[17] Pope, W. B., Sayre, J., Perlina, A., Villablanca, J. P., Mischel, P. S.., Cloughesy, T. F., "MR imaging correlates of survival in patients with high-grade gliomas," AJNR Am. J. Neuroradiol. **26**(10), 2466–2474 (2005).

[18] Gutman, D. A., Cooper, L. A. D., Hwang, S. N., Holder, C. A., Gao, J., Aurora, T. D., Dunn, W. D., Scarpace, L., Mikkelsen, T., et al., "MR imaging predictors of molecular profile and survival: multi-institutional study of the TCGA glioblastoma data set," Radiology **267**(2), 560–569 (2013).

[19] Mazurowski, M. A., Desjardins, A.., Malof, J. M., "Imaging descriptors improve the predictive power of survival models for glioblastoma patients," Neuro-Oncol. **15**(10), 1389–1394 (2013).

[20] McKight, P. E.., Najab, J., "Kruskal-Wallis Test," [The Corsini Encyclopedia of Psychology], John Wiley & Sons, Inc. (2010).

[21] Guo, Y., Hastie, T.., Tibshirani, R., "Regularized linear discriminant analysis and its application in microarrays," Biostatistics **8**(1), 86–100 (2007).

[22] Hall, M., "A decision tree-based attribute weighting filter for naive Bayes," Knowl.-Based Syst. **20**(2), 120–126 (2007).

[23] Coppersmith, D., Hong, S. J.., Hosking, J. R. M., "Partitioning Nominal Attributes in Decision Trees," Data Min. Knowl. Discov. **3**(2), 197–217 (1999).

[24] Hearst, M. A., Dumais, S. T., Osman, E., Platt, J.., Scholkopf, B., "Support vector machines," IEEE Intell. Syst. Their Appl. **13**(4), 18–28 (1998).

[25] Kearns, M.., Ron, D., "Algorithmic Stability and Sanity-Check Bounds for Leave-One-Out Cross-Validation," Neural Comput. **11**(6), 1427–1453 (1999).

[26] Chaddad, A., Zinn, P. O.., Colen, R. R., "Quantitative texture analysis for Glioblastoma phenotypes discrimination," 2014 Int. Conf. Control Decis. Inf. Technol. CoDIT, 605–608 (2014).

[27] Chaddad, A.., Tanougast, C., "High-Throughput Quantification of Phenotype Heterogeneity Using Statistical Features," Adv. Bioinforma. **2015**, e728164 (2015).

[28] Chaddad, A., Zinn, P. O.., Colen, R. R., "Radiomics texture feature extraction for characterizing GBM phenotypes using GLCM," Biomed. Imaging ISBI 2015 IEEE 12th Int. Symp. On, 84–87, IEEE (2015).

[29] Chaddad, A.., Colen, R. R., "Statistical feature selection for enhanced detection of brain tumor," SPIE Opt. Eng. Appl., 92170V – 92170V, International Society for Optics and Photonics (2014).

[30] Toews, M.., Wells III, W. M., "Efficient and robust model-to-image alignment using 3D scale-invariant features," Med. Image Anal. **17**(3), 271–282 (2013).